Intermediate-range Casimir-Polder interaction probed by high-order slow atom diffraction

C Garcion, N Fabre, H Bricha, F Perales, S Scheel, M Ducloy, G Dutier

Intermediate-range Casimir-Polder interaction probed by high-order slow atom diffraction

C. Garcion[1], N. Fabre[1], H. Bricha[1], F. Perales[1], S. Scheel[2], M. Ducloy[1], and G. Dutier[1*]
[1] *Université Sorbonne Paris Nord, Laboratoire de Physique des Lasers, CNRS, (UMR 7538), F-93430, Villetaneuse, France and*
[2] *Institut für Physik, Universität Rostock, Albert-Einstein-Straße 23-24, D-18059 Rostock, Germany*

At nanometer separation, the dominant interaction between an atom and a material surface is the fluctuation-induced Casimir–Polder potential. We demonstrate that slow atoms crossing a silicon nitride transmission nanograting are a remarkably sensitive probe for that potential. A 15% difference between nonretarded (van der Waals) and retarded Casimir–Polder potentials is discernible at distances smaller than 51 nm. We discuss the relative influence of various theoretical and experimental parameters on the potential in detail. Our work paves the way to high-precision measurement of the Casimir–Polder potential as a prerequisite for understanding fundamental physics and its relevance to applications in quantum-enhanced sensing.

The Casimir–Polder (CP) interaction between an atom or molecule and polarizable matter [1] has been intensively studied theoretically as a fundamental electromagnetic dispersion force [2, 3]. It originates from quantum fluctuations of the electromagnetic field that spontaneously polarizes otherwise neutral objects. Interaction strength and spatial dependence are the result of a unique combination of atom species, internal atomic state and material properties and geometry. The Casimir–Polder interaction is part of a larger family of fluctuation-induced electromagnetic forces that also include the well-known Casimir force [4] that has been studied, e.g. between a metallic sphere and a nanostructured surface [5, 6]. Historically, and rather confusingly, the non-retarded regime with $U_{\mathrm{vdw}}(z) = -C_3/z^3$ is sometimes called the van der Waals (vdW) potential in order to distinguish it from retarded (or Casimir-Polder) regime, which asymptotically converges to $U_{\mathrm{ret}}(z) = -C_4/z^4$ at large distance from the surface z.

Pioneering work with Rydberg atoms [7] predominantly probed the non-retarded regime even at atom-surfaces distance as large as 1 μm due to major contributions from atomic transitions in the mid-IR. On the other hand, when the atomic transitions are in visible or near UV regions – such as for atoms in their ground states – the atom-surface interaction will be in the CP regime. This scenario is relevant for ground-state atomic beams [8], cold atoms near atomic mirrors [9] and quantum reflection [10]. Very few experiments thus far have studied the cross-over regime where neither limit holds, typically using an adjustable repulsive dipolar force [11]. Studying atom-surface interactions with reasonable accuracy is of major importance as these fundamental fluctuation-induced interactions have not been yet measured with an accuracy better than 5-10% whatever the experimental approach.

In this Letter, we present our experimental and theoretical investigations of matter-wave diffraction of metastable argon atoms by a transmission nanograting at atom-surface distances below 51 nm. The geometric constraint on the atom-surface distance provided by the two adjacent walls is a major asset that eliminates the quasi-infinite open space over a single surface, similar to an ultrathin vapor cell [14]. Atom-surface interactions have previously been studied using transmission nanogratings with atoms at thermal velocities [12, 13]. Our work shows that, lowering the atomic beam velocity below 26 ms^{-1} opens up new experimental opportunities due to larger interaction times, and produces diffraction spectra dominated by the atom-surface interaction [15]. The precise control of nanograting geometry and experimental parameters related to the atom beam leads us to observe the minute influence of retardation. This paves the way to accurate CP potential measurements that can be compared against detailed theoretical models.

Transmission gratings etched into a 100 nm thick silicon nitride (Si_3N_4) membrane are commonly made using achromatic interferometric lithography (AIL) [16] using UV light, resulting in gratings with pitch down to 100 nm covering areas of several mm^2. For its versatility in nanograting design, we chose electron beam lithography to pattern a new generation of resists with high selectivity during etching and low line edge roughness [17]. A 200 nm-period transmission nanograting has been fabricated on a 100 nm thick membrane of 1×1 mm^2 size. The combination of 100 keV e-beam lithography and anisotropic reactive ion etching ensures parallel walls with deviations smaller than 0.5 degrees from the vertical (see Supp. Mat. for details). The SEM image of a cleaved nanograting shows smooth and anisotropically etched walls, rounded with a 21 nm radius of curvature along the atom propagation axis x (Fig. 1(a) and inset). Statistical analysis of MEB images reveals a slotted hole geometry of the slits (with straight section along 90% of the total slit length), with a main width $W = 102.7 \pm 0.3$ nm and a FWHM distribution of 7 nm (Fig. 1(b)).

Hybrid experiments at the interface between atomic physics and nanoscience often use alkali atoms for convenient laser cooling and manipulation. However, nanostructures chemically react with residual vapor that alters

the CP potential unpredictably [18]. Using noble gas atoms in a metastable state prevents chemical damage on nanostructures while retaining the ability for laser manipulation. The $^3P_2$ metastable state of argon is used for an efficient and accurate time-position detection by microchannel plates with 80 mm diameter in front of a delay line detector (DLD80 from RoentDek Handels GmbH). The experiment starts with a supersonic beam of argon followed by a counterpropagating electron gun, which provides a flux of 10^8 Ar* atoms per second. The cycling transition $^3P_2 \longleftrightarrow {}^3D_3$ ($\Gamma = 2\pi \times 5.8$ MHz, $\lambda = 811.531$ nm) is used by a Zeeman decelerator to trap atoms in a magneto-optical trap (MOT). The trap consists of anti-Helmholtz coils providing the magnetic field and 3 retro-reflected laser beams, red-detuned by 2Γ, with 7 mW total power and 2.54 cm beam diameter. Approximately 10^7 atoms are trapped at a temperature of ≈ 20 mK.

An initial pulse sequence pushes an atom cloud at a chosen velocity orthogonally to the incoming supersonic beam at 13 Hz repetition rate [19]. During this time, the magnetic field remains constant and the molasses laser beams are switched off. Simultaneously, a second laser (5 mW frequency-adjustable laser on the same cycling transition) is turned on for 0.4 ms towards the detector and focussed to 20 cm after the MOT position. Atoms remain in the $m_F = +2$ state without any influence on the diffraction process. A time-of-flight (TOF) measurement is then performed, with the time-position detector 88.5 cm away from the MOT. With this pushing technique, the relative spread of the atomic velocity distribution, $\Delta v/v$, is already less than 10%. Moreover, a time selection of 1 ms is applied to obtain an even narrower velocity distribution. Additionally, for an absolute velocity determination, we used a light chopper with two resonant lasers of 1 mm diameter perpendicular to the atomic beam axis, separated by $\Delta x = 266.5 \pm 1.3$ mm and time triggered with a time sequence accuracy below 50 μs. We obtained mean velocities and respective uncertainties of 19.1 ± 0.2 ms^{-1} and 26.2 ± 0.1 ms^{-1} for both recorded spectra.

The vertical y-axis (see Fig. 1(c)) has been chosen for the slit alignment in order to impose a diffraction expansion perpendicular to the earth's gravitational field. At 56 cm from the MOT, the atomic beam diameter is much larger (≈ 5 cm) than the entire nanograting surface and all slits along the y-axis contribute equally to the signal. This is not the case along the z-axis (diffraction axis) where the angular beam distribution acts as an incoherent source and smears the signal out, in particular interference orders that are separated by more than 2.6 (1.9) mrad for 19.1 (26.2) ms^{-1}. A compromise between atomic flux through the nanograting and fringe visibility (smearing) is achieved with a free opening of $L_g = 306 \pm 5$ μm between the vertical edge of the plate and the nanograting boundary. The atomic beam divergence, $\Delta_\theta^{\text{beam}}$, through the 306 μm slit at a distance L_1 from the MOT fits a Gaussian profile with 1.4 mrad FWHM. As a consequence, the beam divergence alters perceptibly the measured diffraction spectra, but in a controlled way. The nanograting is fixed on a 6D piezo system (SmarPod 11.45 from SmarAct GmbH) to ensure a 90.0 ± 0.1 degree angle between the atomic beam and the z-axis on the nanograting. An angular deviation as small as 0.2 degrees introduces noticeable asymmetry of the intensities of the diffraction orders.

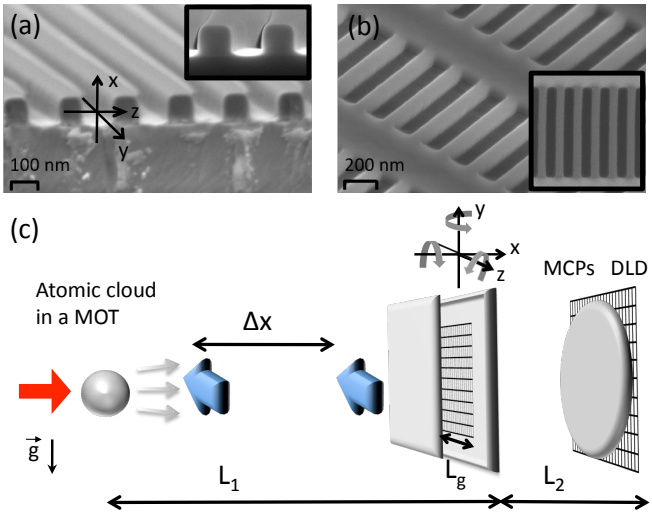

FIG. 1. SEM images of (a) a cleaved nanograting on a substrate and (b) a free standing membrane. (c) Experimental set-up. An atomic cloud is periodically pushed from a MOT at a chosen velocity through a nanograting $L_1 = 56$ cm away. A time-position detector is located $L_2 = 308$ mm behind the nanograting.

Two experimental diffraction spectra are shown in Fig. 2 for contributing velocities between $18.7 \ldots 19.5$ ms^{-1} and $25.5 \ldots 26.9$ ms^{-1}. Small electronic aberrations in position have been corrected by the use of a 2600-hole grid pattern, and no intensity inhomogeneity has been noticed at the experimental accuracy level. The recording times were 40 and 13 hours for 1.006×10^5 and 1.512×10^5 atoms, respectively. In general, for matter waves propagating through a transmission grating, the diffraction spectrum envelope is determined by the wavelength and the single slit width, while the interference peak visibility stems from the transverse coherence length of the source. In the present situation, the nanograting slit width effectively narrows due to atoms that are close enough to a surface being mechanically attracted and deflected by the Casimir–Polder potential. Metastable atoms colliding the surface at room temperature are scattered randomly at high velocity, and will return to their ground state [20].

For atoms at thermal velocities, the region near the surfaces the atoms needed to avoid was assumed to be a few nanometers [12, 13]. Using classical trajectories,

we can estimate a lower limit for the distance at which the atoms can pass the nanobars to be $d_0 = 16.2\,(14.2)$ nm at a beam velocity of $19.1\,(26.2)$ ms^{-1} or, equivalently, an effective slit width of $W_{\rm eff} = 70.3\,(74.3)$ nm. Such a major reduction cannot be neglected when explaining experimental diffraction spectra ($\lambda_{\rm dB}/W_{\rm eff} = 14$ mrad at 19.1 ms^{-1}). The fringe visibility depends only on the transverse coherence length of the atomic beam, $L_c = \lambda_{\rm dB} L_1/a$, with a the diameter of the incoherent source, as given by the van Cittert–Zernike theorem [22]. However, the quadratic dispersion relation for matter waves suppresses the dephasing compared to light [23], and hence enlarges L_c. From the cloud size in the MOT, $a = 330 \pm 40$ μm, followed by thermal expansion, one finds $L_c = 560 \pm 45$ (380 ± 30) nm at 19.1 (26.2) ms^{-1} beam velocity.

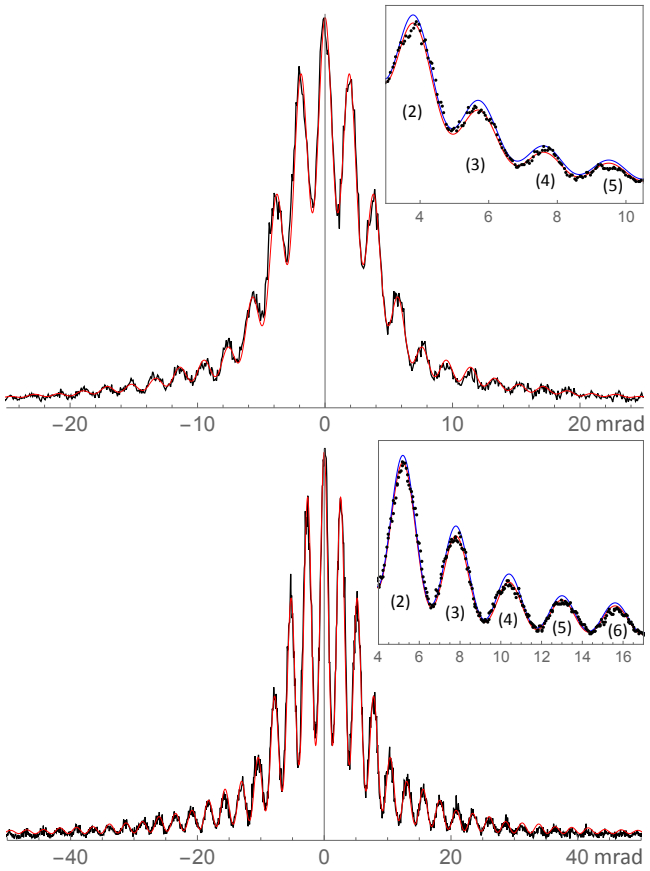

FIG. 2. Experimental diffraction spectra for beam velocities of 26 ms^{-1} (top) and 19.1 ms^{-1} (bottom) in black. The red curves are theoretical spectra with a single adjustable parameter (d_0). The insets show individual diffraction orders. Black dots result from experimental spectra averaged over positive and negative diffraction orderes. Red (blue) curves are calculated with retarded CP (non-retarded vdW) potentials.

The Huygens-Kirchhoff principle can be utilized for atoms propagating in a potential that is small compared to their kinetic energy [24, 25]. This can be justified with the help of the effective slit approximation, which removes atoms with potential energies that are too large. Additionally, the detection in the far field validates the Fraunhofer approximation ($x \gg W_{\rm eff}^2/\lambda_{\rm dB}$), in which the diffraction pattern results from the sum of wave path differences at the nanograting output. The CP potential is included in the wave propagation as an additional phase $\Phi_{\rm CP}(z)$ that depends on the atom-surface distance inside the nanograting slit z. In short, the total phase can be written as $F(z,\theta) = kz\sin\theta + \Phi_{\rm CP}(z)$ for an incidence angle θ and a wave number k. The incoming Gaussian wave packets have a standard deviation $\sigma_{\rm coh} = L_c/2$ [26, 27]. The experimental value for L_c covers up to 7 slits coherently and hence, the beam cannot be considered as a plane wave. The diffraction intensity then reads as

$$I(\theta) = \left| \sum_{\rm slits} \int_{W_{\rm eff}} \exp\left[iF(z',\theta)\right] \exp\left[-\frac{z'^2}{2\sigma_{\rm coh}^2}\right] dz' \right|^2 . \quad (1)$$

In eikonal approximation, the phase shift imprinted by a potential $U_{CP}(z)$ is the integral of the potential along the particle trajectory [28]. Neglecting the surface potential outside the grating, one finds

$$\Phi_{\rm CP}(z) = -\frac{1}{\hbar v}\int_0^L U_{CP}(x,z)dx \quad (2)$$

where $L = 100$ nm is the nanograting depth and v the beam velocity. However, it is necessary to account for the exact shape of the grating along the x-axis, because the slit widths increase near the output. We incorporate this effect by using a smaller slit thickness of $L_{\rm eff} = 95$ nm.

In pioneering experiments with nanogratings and supersonic beams [12, 29], the CP potential is modelled in the non-retarded regime as $U_{\rm vdw}(z) = -C_3^{\rm nr}/z^3$ for the two adjacent surfaces. Semi-infinite surfaces are implicitly considered everywhere inside the grating even if though this is not correct near the edges. Further, the effect of multiple reflection from the bar opposite has been neglected [30]. These approximations are justified for fast atoms or molecules as the overall phase shift remains small on average [31]. In the non-retarded regime, the coefficient $C_3^{\rm nr}$ is given by the Lifshitz formula [34, 35]

$$C_3^{\rm nr} = \frac{\hbar}{16\pi^2\epsilon_0}\int_0^\infty \alpha(i\xi)\frac{\epsilon(i\xi)-1}{\epsilon(i\xi)+1}d\xi \quad (3)$$

where $\alpha(i\xi)$ denotes the atomic dynamic polarizability, and $\epsilon(i\xi)$ is the surface permittivity taken at imaginary frequencies $i\xi$. For metastable argon in the ^{3}P$_2$ state, we obtain $C_3^{\rm nr} = 1.25$ a.u., or 5.04 meV nm^3 in front of a Si_3N_4 surface with spectral responses in the UV and IR [33]. An estimate of the uncertainty of this value is rather difficult to obtain. First, the material may show imperfections with regard to its fabrication and size [32] that alter the index of refraction. Second, the electronic structure of argon in the ^{3}P$_2$ metastable state, due to its

11.5 eV internal energy, makes the potential more sensitive to the material optical response in the visible and near-UV regions, where accurate optical response data are difficult to obtain. Third, the electronic core contribution has been estimated to be in the range of 0.03 a.u. using the first ionic state. Such a small core contribution is a clear theoretical advantage of metastable argon compared to heavier (alkali) atoms [36]. The temperature dependence of $C_3^{\rm nr}$ can be safely neglected here, in contrast to situations in which dominant transitions appear in the mid-IR region [21]. Altogether, we conservatively estimate a 10% uncertainty that is similar to other CP calculations.

The improvement in experimental accuracy allows us to discern the non-retarded regime and the onset of retardation effects, that arise due to the finite field propagation time between atom and surface. This effect becomes relevant at distances larger than $\lambda_{\rm opt}/(2\pi)$. Without resorting to a full calculation of the exact shape of the potential, one can resort to sophisticated interpolations. Here, we use a model derived in Ref. [37] that is built on a single atomic transition (here, $\lambda_{\rm opt} = 811.5$ nm for Ar $^3{\rm P}_2$), for which the effective coefficient $C_3^{\rm eff}(z)$ reads as

$$C_3^{\rm eff}(z) = C_3^{\rm nr}\left[\zeta + (2-\zeta^2)f_1(z) + 2\zeta f_2(z)\right]/\pi \qquad (4)$$

with $\zeta(z) = 2z(2\pi)/\lambda_{\rm opt}$ and $f_i(z)$ given in [38]. This expression provides an interpolation between $U_{\rm vdw} \propto z^{-3}$ at short distances and $U_{\rm ret} \propto z^{-4}$ for $z \gg \lambda_{\rm opt}$. Inside the grating, $C_3^{\rm eff}(z)$ goes from $C_3^{\rm nr}$ at $z = 0$ to $C_3^{\rm eff}(51\ {\rm nm}) = 0.78\ C_3^{\rm nr}$ (Fig. 3(a)). On average, the detected atoms will have experienced $\langle C_3^{\rm eff}\rangle = 0.85\ C_3^{\rm nr}$, which corresponds to a 15% deviation from the non-retarded regime. This model is in very good agreement with the complete QED calculation [2] to within a few percent for semi-infinite surfaces, and arguably much faster to calculate.

As first shown in Ref. [13], the fitting procedure is extremely sensitive to the grating geometry, and there is no unique relation between the experimental spectrum and the set of possible theoretical parameters. A chi-squared test is used with $\chi^2 = \sum_\theta (I_\theta^{\rm exp} - I_\theta^{\rm theo})^2/\sigma_{\theta,{\rm exp}}^2$, where $\sigma_{\theta,{\rm exp}}$, $I_\theta^{\rm exp}$ and $I_\theta^{\rm theo}$ are the experimental noise standard deviation, and the experimental and theoretical intensities at the angle θ, respectively. Indeed, we find a linear relation between potential strength and slit width as well as nanograting thickness L_{ng} to within 10% of their nominal values: $\Delta W = \pm 1$ nm $\rightarrow \Delta C_3^{\rm nr} = \pm\ 0.07$ a.u. and $\Delta L_{ng} = \pm 10$ nm $\rightarrow \Delta C_3^{\rm nr} = 0.16$ a.u. On the other hand, $\sigma_{\rm coh}$ and $\Delta_\theta^{\rm beam}$ are not linked to any other parameters. The remaining important parameter, $W_{\rm eff} = W - 2d_0$ in Eq. (1), is the maximum additional CP phase shift with $\Phi_{CP}^{\rm max} = \Phi_{CP}(d_0)$. Note that $\Phi_{CP}^{\rm max}$ is different for both models as d_0 increases with larger $C_3^{\rm nr}$. Also, at larger velocities this parameter was not considered to be critical [11].

With this, we can discuss the variations of $C_3^{\rm nr}$ and $\Phi_{CP}^{\rm max}$. Figure 3(b) shows the $(\chi^2_{\rm min} + 40\sigma)$-surfaces for a beam velocity of 26.2 ms^{-1}, where $\sigma = 6.2$ is the standard deviation for two parameters. The magnification of 40σ has been chosen merely for clarity. The dashed line is the calculated expected $C_3^{\rm nr}$. Four different minima have been found: $\Phi_{CP}^{\rm max} = 4.5, 10.5, 17.5, 22$ rad for $z \approx 17.5, 13.1, 11.0, 10.1$ nm from the surface. $\Phi_{CP}^{\rm max} = 10.5$ rad gives the smallest χ^2 for both models. Figure 3(c) shows the $(\chi^2_{\rm min} + \sigma)$-contours proving the importance of the full CP potential (red) and rejecting the nonretarded approximation (blue). For further clarity, the insets in Fig. 2 emphasizes the influence of both models on the spectra calculated at $\Phi_{CP}^{\rm max} = 10.5$ rad with the theoretically expected $C_3^{\rm nr}$. Note that our extracted experimental value of $C_3^{\rm nr} = 1.24 \pm 0.15$ a.u. also corrects the rather crude approximation given in Ref. [40].

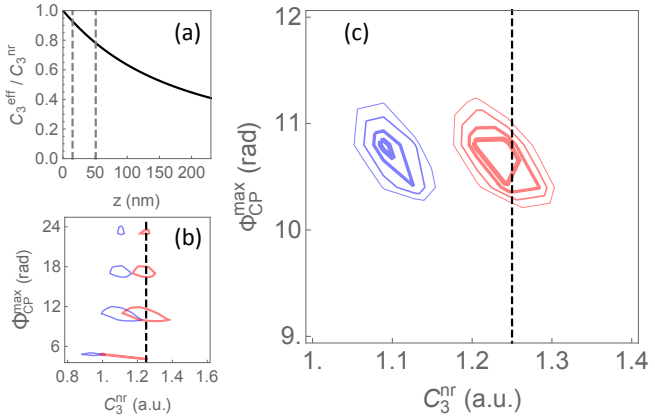

FIG. 3. (a): $C_3^{\rm eff}/C_3^{\rm nr}$ as function of atom-surface distance. (b),(c): $\chi^2_{min} + n\sigma$ [n=40 (b), n =1, 3, 6, 9 (c)] as functions of $C_3^{\rm nr}$ and $\Phi_{CP}^{\rm max}$ at 26.2 ms^{-1} for nonretarded vdw (blue) and retarded CP (red) potentials. The dashed line shows the theoretical value for $C_3^{\rm nr}$.

The advantage of using a slow atomic beam with a well-defined velocity rather than a thermal beam derives from the fact that the atom-surface interaction potential can be probed to a much higher accuracy. However, this presents another difficulty: the Kirchhoff approximation stipulates that the (change of the) transverse wavenumber has to be small compared to the longitudinal wavenumber, $k_{\rm perp}/k \ll 1$ [41]. The slower the atoms become, the more (relative) transverse momentum they accumulate whilst traversing the grating. At the cut-off that determines the effective slit width, we can estimate the relative change in transverse wavenumber to be roughly 5% for a beam velocity of 26.2 ms^{-1}, but already 10% for a velocity of 19.1 ms^{-1}. This implies that the Kirchhoff approximation can no longer be relied upon at slower beam velocities, at which a more detailed theoretical description is required.

In conclusion, we have demonstrated the importance of the retarded Casimir-Polder potential for the diffraction of metastable Ar in a range of atom-surface distances

as small as $\approx 15 \ldots 51$ nm with a Si_3N_4 transmission nanograting. Due to atomic velocities as slow as 19.1 ms^{-1} as well as an accurate geometrical characterization of the nanograting, we were able to discriminate a difference in the CP potential as small as 15%. For lower velocities or smaller slit widths, the semiclassical model utilized for the simulations should be replaced by a quantum mechanical model. Such a theoretical refinement will introduce quantum reflexion at the slit walls and may produce, in some geometry, gravity Q-bounces as found for neutrons [42]. This work opens the opportunity for unprecedented and accurate CP potential measurements by controlling the tilt of the nanograting, which, combined with tomography methods, would lead to a thorough understanding of atom-surface interactions with implications for theoretical physics as well as nano metrology. For example, the hypothetical non-Newtonian fifth force [43] could be constrained by an atomic physics experiment. Atomic quantum random walks [44] based on multi-path beam splitters can be simply realized with two or more nanogratings, and closed-loop interferometers can be made extraordinary compact.

The authors from Laboratoire de Physique des Lasers acknowledge the "Institut Francilien de Recherche sur les Atomes Froids" (IFRAF) and the Domaine d'Intérêt Majeur "Science et Ingénierie en Région Île-de-France pour les Technologies Quantiques" (SIRTEQ) for supports. The work was partly supported by the French Renatechnetwork. The authors acknowledge B. Darquié for fruitful data analysis discussions.

* dutier@univ-paris13.fr

[1] H.B.G. Casimir and D. Polder, *The influence of retardation on the London-van der Waals forces*, Phys. Rev. **73**, 360 (1948).

[2] S. Scheel and S. Y. Buhmann, *Macroscopic quantum electrodynamics – concepts and applications*, Acta Phys. Slovaca **58**, 675 (2008).

[3] S. Y. Buhmann, *Dispersion Forces I – Macroscopic Quantum Electrodynamics and ground-state Casimir, Casimir–Polder and van der Waals forces* (Springer, Berlin, 2012).

[4] H.B.G. Casimir, *On the Attraction between Two Perfectly Conducting Plates*, Proc. Kon. Ned. Akad. Wet. **51**, 793 (1948).

[5] U. Mohideen and A. Roy, *Precision Measurement of the Casimir Force from 0.1 to 0.9 μm*, Phys. Rev. Lett. **81**, 4549 (1998).

[6] F. Intravaia, *et al.*, *Strong Casimir force reduction through metallic surface nanostructuring*, Nat. Commun. **5**, 2515 (2013).

[7] V. Sandoghdar, C.I. Sukenik, E.A. Hinds, and S. Haroche, *Direct measurement of the van der Waals interaction between an atom and its images in a micron-sized cavity*, Phys. Rev. Lett. **68**, 3432 (1992).

[8] C. I. Sukenik, M. G. Boshier, D. Cho, V. Sandoghdar, and E. A. Hinds, *Measurement of the Casimir–Polder force*, Phys. Rev. Lett. **70**, 560 (1993).

[9] A. Landragin , J.-Y. Courtois, G. Labeyrie, N. Vansteenkiste, C. I. Westbrook and A. Aspect, *Measurement of the van der Waals Force in an Atomic Mirror*, Phys. Rev. Lett. **77**, 1464 (1996).

[10] F. Shimizu, *Specular Reflection of Very Slow Metastable Neon Atoms from a Solid Surface*, Phys. Rev. Lett. **86**, 987 (2001).

[11] H. Bender, Ph. W. Courteille, C. Marzok, C. Zimmermann, and S. Slama, *Direct Measurement of Intermediate-Range Casimir-Polder Potentials*, Phys. Rev. Lett. **104**, 083201 (2010).

[12] R. E. Grisenti, W. Schöllkopf, J. P. Toennies, G. C. Hegerfeldt, and T. Köhler, *Determination of Atom-Surface van der Waals Potentials from Transmission-Grating Diffraction Intensities*, Phys. Rev. Lett. **83**, 1755 (1999); R. Brühl, P. Fouquet, R. E. Grisenti, J. P. Toennies, G. C. Hegerfeldt, T. Köhler, M. Stoll, and C. Walter, *The van der Waals potential between metastable atoms and solid surfaces: Novel diffraction experiments vs. theory*, Europhys. Lett. **59**, 357 (2002).

[13] V. P. A. Lonij, W. F. Holmgren, and A. D. Cronin, *Magic ratio of window width to grating period for van der Waals potential measurements using material gratings*, Phys. Rev. A **80**, 062904 (2009).

[14] M. Fichet, G. Dutier, A. Yarovitsky, P. Todorov, I. Hamdi, I. Maurin, S. Saltiel, D. Sarkisyan, M.-P. Gorza, D. Bloch, and M. Ducloy, Exploring the van der Waals atom-surface attraction in the nanometric range, Europhys. Lett. **77**, 54001 (2007).

[15] S. Nimmrichter and K. Hornberger, *Theory of near-field matter-wave interference beyond the eikonal approximation*, Phys. Rev. A **78**, 023612 (2008).

[16] T. A. Savas, S. N. Shah, M. L. Schattenburg, J. M. Carter, and H. I. Smith, *Achromatic interferometric lithography for 100-nm-period gratings and grids*, J. Vac. Sci. Technol. B **13**, 2732 (1995); T. A. Savas, M. L. Schattenburg, J. M. Carter, and H. I. Smith, *Large-area achromatic interferometric lithography for 100 nm period gratings and grids*, J. Vac. Sci. Technol. B **14**, 4167 (1996).

[17] S. Thoms and D. S. Macintyre, *Investigation of CSAR 62, a new resist for electron beam lithography*, J. Vac. Sci. Technol B **32**, 06FJ01 (2014).

[18] J. M. McGuirk, D. M. Harber, J. M. Obrecht, and E. A. Cornell, *Alkali-metal adsorbate polarization on conducting and insulating surfaces probed with Bose-Einstein condensates*, Phys. Rev. A **69**, 062905 (2004).

[19] T. Taillandier-Loize *et al.*, *A simple velocity-tunable pulsed atomic source of slow metastable argon*, J. Phys. D: Appl. Phys. **49**, 135503 (2016).

[20] H. D. Hagstrum, *Theory of Auger ejection of electron from metal by ions*, Phys. Rev. **96**, 336 (1954).

[21] A. Laliotis, T. Passerat De Silans, I. Maurin, M. Ducloy, and D. Bloch, *Casimir-Polder interactions in the presence of thermally excited surface modes*, Nat. Commun. **5**, 4364 (2014).

[22] M. Born and E. Wolf, *Principles of optics*, 4th. ed. (Pergamon Press, 1970).

[23] B. Taylor, K.J. Schernthanner, G. Lenz, and P. Meystre, The van Cittert-Zernike theorem in atom optics, Opt. Commum. **110**, 569 (1994).

[24] R. Feynman, *Space-Time Approach to Non-Relativistic Quantum Mechanics*, Rev. Mod. Phys. **20**, 367 (1948).

[25] A. L. Kholodenko and L. H. Kauffman, *Huygens triviality of the time-independent Schr?dinger equation. Applications to atomic and high energy physics*, Ann. Phys. **390**, 1 (2018).

[26] A. Zecca, *Double Slit Diffraction Pattern of Gaussian Wave Packet Interacting with the Wall*, Adv. Studies Theor. Phys. **1**, 539 (2007).

[27] B. J. Thompson and E. Wolf, *Two-Beam Interference with Partially Coherent Light*, J. Opt. Soc. Am. **47**, 10 (1957).

[28] L. Landau and E. Lifchitz, *Quantum Mechanics: Non-Relativistic Theory*, 3th. ed. (Pergamon Press, 1974).

[29] J. D. Perreault and A. D. Cronin, *Observation of Atom Wave Phase Shifts Induced by Van Der Waals Atom-Surface Interactions*, Phys. Rev. Lett. **95**, 133201 (2005).

[30] G. Dutier, S. Saltiel, D. Bloch, and M. Ducloy, *Revisiting optical spectroscopy in a thin vapor cell: mixing of reflection and transmission as a Fabry?Perot microcavity effect*, J. Opt. Soc. Am. B **20**, 793 (2003).

[31] C. Brand, J. Fiedler, T. Juffmann, M. Sclafani, C. Knobloch, S. Scheel, Y. Lilach, O. Cheshnovsky, and M. Arndt, *A Green's function approach to modeling molecular diffraction in the limit of ultra-thin gratings*, Ann. Phys. **527**, 580 (2015).

[32] S. Zollner and E. Apen, *Optical Constants for Metrology of Hydrogenated Amorphous Silicon-Nitrogen Alloys on Si*, AIP Conference Proceedings **550**, 532 (2001); C. J. Krückel, A. Fülöp, Z. Ye, P. A. Andrekson, and V. Torres-Company, *Optical bandgap engineering in nonlinear silicon nitride waveguides*, Opt. Exp. **25**, 15370 (2017).

[33] H. R. Philipp, *Optical Properties of SiliconNitride*, J. Electrochem. Soc. **120**, 295 (1973); K. Luke, Y. Okawachi, M. R. E. Lamont, A. L. Gaeta, and M. Lipson, *Broadband mid-infrared frequency comb generation in a Si_3N_4 microresonator*, Opt. Lett. **40**, 4823 (2015).

[34] E. M. Lifshitz, *The theory of molecular attractive forces between solids*, Sov. Phys. JETP, **2**, 73 (1956).

[35] C. Mavroyannis, *The interaction of neutral molecules with dielectric surfaces*, Mol. Phys. **6**, 593 (1963).

[36] A. Derevianko, W. R. Johnson, M. S. Safronova and J. F. Babb, *High-Precision Calculations of Dispersion Coefficients, Static Dipole Polarizabilities, and Atom-Wall Interaction Constants for Alkali-Metal Atoms*, Phys. Rev. Lett. **82**, 3589 (1999); A. D. Cronin and J. D. Perreault, *de Broglie Wave Phase Shifts Induced by Surfaces Closer than 25 nm*, J. Phys.: Conf. Series **19**, 48 (2005).

[37] J. M. Wylie and J. E. Sipe, *Quantum electrodynamics near an interface*, Phys. Rev. A **30**, 1185 (1984).

[38] $f_1(z) = Ci(\zeta)\sin(\zeta) - (Si(\zeta) - \pi/2)\cos(\zeta)$ and $f_2(z) = -Ci(\zeta)\cos(\zeta) - (Si(\zeta) - \pi/2)\sin(\zeta)$ where $Ci(z)$ and $Si(z)$ are the integral cosine and sine functions

[39] W. H. Press, S. Teukolsky, W. Vetterling, and B. Flannery, *Numerical Recipes* (Cambridge University Press, Cambridge, 2007)

[40] J.-C. Karam, N. Wipf, J. Grucker, F. Perales, M. Boustimi, G. Vassilev, V. Bocvarski, C. Mainos, J. Baudon, and J. Robert, *Atom diffraction with a 'natural' metastable atom nozzle beam*, J. Phys. B: At. Mol. Opt. Phys. **38**, 2691 (2005).

[41] D. Arsenović, M. Božić, O. V. Man'ko, and V. I. Man'ko, *Equivalence of two forms of the solution to the Schrödinger equation for a particle passing through a grating*, J. of Russian Laser Res. **26**, 94 (2005).

[42] T. Jenke, P. Geltenbort, H. Lemmel, and H. Abele, *Realization of a gravity-resonance-spectroscopy technique*, Nat. Phys. **7**, 468 (2011).

[43] I. Antoniadis *et al.*, *Short-range fundamental forces*, C. R. Physique **12**, 755 (2011).

[44] M. Karski, L. Förster, J-M. Choi, A. Steffen, W. Alt, D. Meschede and A. Widera, "Quantum Walk in Position Space with Single Optically Trapped Atoms", Science **325** 174 (2009)